Proceeding Paper

Molecular Analysis of Glu-Ureido Template via DFT[†]

Mohd. Faheem [1,2], Vaibhav Pandey [1], Anjli Shrivastav [1], Manisha Prasad [2,*] and Manish Dixit [1,*]

[1] Department of Nuclear Medicine, Sanjay Gandhi Postgraduate Institute of Medical Sciences, Lucknow 206014, UP, Indiafaheemurfi@gmail.com (M.F.); vaibhavparasar94@gmail.com (V.P.); anjliknipss@gmail.com (A.S.)

[2] Department of Chemistry, University of Lucknow, Lucknow 226007, UP, India

* Correspondence: sharmamanisha1@rediffmail.com (M.P.); dixitm@sgpgi.ac.in (M.D.)

[†] Presented at the 28th International Electronic Conference on Synthetic Organic Chemistry (ECSOC 2024), 15-30 November 2024; Available online: https://sciforum.net/event/ecsoc-28.

Abstract: The Prostate cancer (PC) is a major problem all over worldwide and this is the second highest cancer-related mortality rate after lung cancer all over worldwide. At least 299,010 likely cases in men were reported in the US in 2024 and about 35,250 deaths are reported. The overexpression of prostate-specific membrane antigen (PSMA) is a key factor in the progression of prostate cancer and contributes to metastasis in lymph nodes, soft tissues and bones metastasis. The numerous studies have reported that, Glu-ureido-based molecules exhibit high binding affinity for PSMA. The earliest imaging agents developed from this structure were labeled with radioactive halogen isotopes and demonstrated nanomolar binding affinity, leading to exceptional imaging properties. Hence the Glu-ureido chemical moiety is a very important template as inhibitor of PSMA. In this study to explore the chemical structural and electronic features of Glu-Ureido structure with the aid of quantum chemistry computer simulations. In this study, first optimized the structure of this chemical structure using the B3LYP 6311-G (++, d, p) basis set. In this study investigated the maximal quantity of electronic charge transfer (N_{max}), chemical hardness (η), electrostatic potential, chemical potential (μ) and electrophilicity (ω). By the using Natural Bond Orbital (NBO) analysis, the examination shows that the molecule's chemically active regions π-electron-electron delocalization within the molecule that contribute to its stability.

Keywords: Glu-ureido; DFT; prostate cancer; PSMA

1. Introduction

The (((*R*)-5-amino-1-carboxypentyl)carbamoyl)-*D*-glutamic acid (Glu-Ureido), is a synthetic chemical of glutamic acid derivatives, which is the site-specific chemical moiety for prostate cancer patients [1]. This template features a distinct structure characterized by the presence of an *R*-configured amino carboxypentyl group attached to the carbamoyl moiety of *D*-glutamic acid (Table 1) [2]. The Glu-Ureido is particularly notable for its potential applications in radiopharmaceutical research as an imaging agent as well as therapy in prostate cancer patients, where it serves as a key intermediate in the synthesis of Prostate Specific Membrane Antigen (PSMA) based molecular architectures and bioactive compounds [3]. The Glu-Ureido scaffold serves as the foundation for a variety of PSMA-based inhibitors due to its high affinity and specificity for PSMA, facilitating the progress of advanced diagnostic and therapeutic agents for prostate carcinoma [2–6].

The PSMA is a cell surface enzyme overexpressed in prostate adenocarcinoma, making it a critical biomarker and therapeutic target [9]. The active part of the Glu-Ureido scaffolds that participates in inhibiting PSMA are primarily the urea linkage of lysin and glutamic acid [6,7]. The glutamic acid portion mimics the natural substrate of PSMA, enabling the scaffold to bind effectively to the enzyme's active site. The urea linkage plays a crucial role in enhancing the binding affinity and specificity of the inhibitor by providing

Chem. Proc. **2024**, *6*, x FOR PEER REVIEW

2 of 10

additional interactions with the enzyme [8]. This strategic combination allows the Glu-Ureido scaffold to engage in key interactions with the amino acid residues within the PSMA active site. These interactions typically include hydrogen bonding, electrostatic interactions and hydrophobic contacts, which collectively contribute to the high binding affinity and inhibitory potency of the scaffold [8–10]. In this article to apply the DFT to better understand behaviour with the receptor by the physical property of the Glu-Ureido chemical moiety.

Table 1. Chemical properties of Glu-Ureido chemical structure.
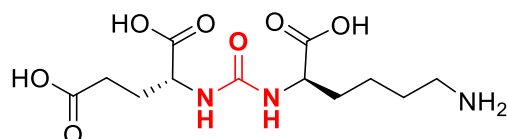
(((*R*)-5-amino-1-carboxypentyl)carbamoyl)-*D*-glutamic acid

B.P. (K)	M.P. (K)	Critical Temp. (K)	Critical Pres. (bar)	Critical Vol (cm³/mol)	Gibbs Energy (KJ/mol)	LogP	tPSA	CLogP	LogS	pKa
1157.4	978.4	1067.7	27.5	859.5	−889.7	−2.1	179.05	−3.49	−0.59	3.29, 4.30, 3.36

A computer quantum mechanical modeling technique, DFT is used to look into molecules' electrical structures, particularly useful in studying complex bioactive compounds like Glu-Ureido linkage. Applying DFT to Glu-Ureido enables researchers to understand its electronic properties reactivity and interaction mechanisms with PSMA. Through DFT calculations, one can gain insights into the compound's molecular orbitals, electron density distribution and potential energy surfaces. This information is crucial for optimizing the design of PSMA inhibitors, as it allows for the prediction of how modifications to the Glu-Ureido scaffold might affect its binding affinity and inhibitory potency. By leveraging DFT, scientists can streamline the development process of PSMA-targeted therapies, enhancing their efficacy and specificity in prostate cancer treatment. As ab-initio studies continues to evolve, more accurate and detailed models of Glu-Ureido interactions with PSMA can be developed. This study will enable a deeper understanding of the electronic and structural factors that govern binding affinity and specificity.

2. Materials and Methods

Ab Initio Computational Calculation

The (((*R*)-5-amino-1-carboxypentyl)carbamoyl)-*D*-glutamic acid (Glu-Ureido) chemical structure was first drawn in ChemDraw software and saved as a .cdx file format. The three-dimensional models was constructed using Chem3D software. Subsequently, the structure was pre-optimized by the universal force field (UFF) in the Avogadro program [11]. The Glu-Ureido quantum chemical calculations were carried out by DFT using B3LYP and 6311-G (++, d, p) basic in Gaussian 09W programme suite [12–16]. The Gaussview 6.0 software [15,16] was used to determine molecular electrostatic potential surfaces, UV-spectra and optimized geometrical parameters. The electric dipole moments (μ), first-order hyperpolarizability (β) and polarizability (α) values were calculated on the previously optimized geometries by using the finite field method (FF) [17–19].

3. Results and Discussion

3.1. Optimized Chemical Skeleton Parameters

The determining a computationally feasible theory level is a critical step in molecular modeling in order to explain the physical features results in good equilibrium geometries, which align with the molecular geometries obtained experimentally for a potent scaffold targeting a specific site. In this sense, the present work decided to evaluate the physical properties by using DFT. Using this theory in relation to the basic functions 6311-G (++,d,p) in order to perform the calculations for molecular optimization. The geometric features of the Glu-Ureido chemical structure were reasonably characterized by this fundamental set combination (Figure 1).
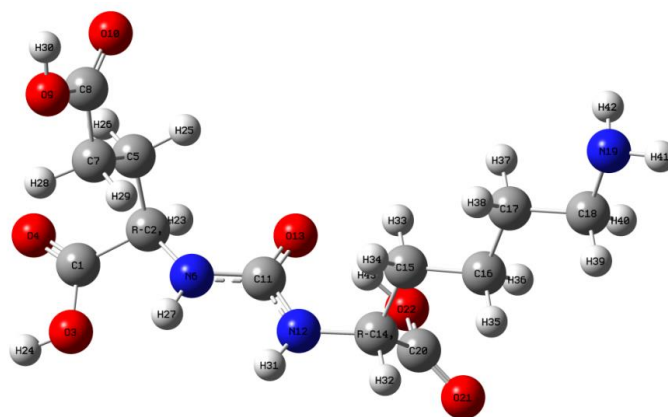
Figure 1. Optimized Glu-Ureido Chemical Structure View.

The Table 2 shows the theoratical data of bond lengths, bond angles and dihedral angle values of the Glu-Ureido chemical moiety theoretically calculated by a given basic set. The Glu-Ureido structure shows C1 point group symmetry. Figure 1 indicates the optimized Glu-Ureido molecular structure, while Table 2 lists the bond parameter values (theoretically).

Table 2. bonds parameter of the optimized Glu-Ureido skeleton.

Bond Length (A°)		Bond Angle (°)		Dihedral Angle (°)	
Atoms Connectivity	**B3LYP**	**Atoms Connectivity**	**B3LYP**	**Atoms Connectivity**	**B3LYP**
C2C1	1.526	O3C1C2	113.506	O4C1C2O3	123.448
O3C1	1.345	O4C1C2	123.043	C5C2C1O3	−128.212
O4C1	1.205	C5C2C1	110.661	N6C2C1C5	113.209
C5C2	1.544	N6C2C1	112.374	C11N6C2C1	139.891
N6C2	1.457	C11N6C2	121.104	C7C5C2C1	66.365
C11N6	1.362	C7C5C2	113.593	C8C7C5C2	174.749
C7C5	1.527	C8C7C5	112.885	O9C8C7C5	176.801
C8C7	1.511	O9C8C7	111.262	O10C8C7O9	122.74
O9C8	1.35	O10C8C7	125.998	N12C11N6C2	−170.56
O10C8	1.207	N12C11N6	116.468	O13C11N6N12	122.231
N12C11	1.362	O13C11N6	121.299	C14N12C11N6	−165.519
O13C11	1.247	C14N12C11	124.945	C20C14N12C11	−70.661
C14N12	1.472	C20C14N12	113.469	C15C14N12C20	111.687
C20C14	1.543	C15C14N12	112.893	C16C15C14N12	171.736
C15C14	1.545	C16C15C14	113.794	C17C16C15C14	−175.901
C16C15	1.533	C17C16C15	112.325	C18C17C16C15	−179.36

Chem. Proc. **2024**, *6*, x FOR PEER REVIEW

4 of 10

C17C16	1.532	C18C17C16	113.117	N19C18C17C16	−177.917
C18C17	1.529	N19C18C17	110.733	O22C20C14N12	53.82
N19C18	1.472	O22C20C14	117.038	O21C20C14O22	121.537
O22C20	1.332	O21C20C14	121.364	H23C2C1C5	107.029
O21C20	1.21	H23C2C1	105.817	H25C5C2C7	109.987
H23C2	1.093	H25C5C2	107.477	H26C5C2C7	110.19
H25C5	1.091	H26C5C2	108.129	H27N6C2C11	119.479
H26C5	1.091	H27N6C2	117.913	H28C7C5C8	107.378
H27N6	1.008	H28C7C5	111.811	H29C7C5C8	107.167
H28C7	1.095	H29C7C5	111.113	H31N12C11C14	115.574
H29C7	1.095	H31N12C11	118.302	H32C14N12C15	108.495
H31N12	1.008	H32C14N12	105.154	H33C15C14C16	110.047
H32C14	1.089	H33C15C14	109.476	H34C15C14C16	109.514
H33C15	1.093	H34C15C14	106.803	H35C16C15C17	109.366
H34C15	1.095	H35C16C15	109.414	H36C16C15C17	109.284
H35C16	1.097	H36C16C15	110.013	H37C17C16C18	109.011
H36C16	1.095	H37C17C16	109.306	H38C17C16C18	108.609
H37C17	1.098	H38C17C16	110.075	H39C18C17N19	107.759
H38C17	1.096	H39C18C17	109.197	H40C18C17N19	113.323
H39C18	1.096	H40C18C17	109.033	H24O3C1C2	179.702
H40C18	1.102	H24O3C1	108.026	H30O9C8C7	179.545
H24O3	0.971	H30O9C8	107.559	H41N19C18C17	177.261
H30O9	0.97	H41N19C18	109.427	H42N19C18H41	105.495
H41N19	1.016	H42N19C18	109.132	H43O22C20C14	−5.235
H42N19	1.017	H43O22C20	110.328	---	---

3.2. Electronic Properties

The molecular boundary orbitals, or HOMO and LUMO, are known to be significant plays in chemical reaction activity. During a chemical reaction, the Lowest Unoccupied Molecular Orbital (LUMO) acts as an electron density acceptor and the Highest Occupied Molecular Orbital (HOMO) primarily roles as an electron donor. The difference between the HOMO and LUMO energies is known as the frontier energy gap, indicated by ΔE_{gap}, and describes a molecular system's hardness or softness, kinetic stability, optical polarizability and chemical reactivity. In general, low kinetic stability and high chemical reactivity (soft electronic systems) are linked to low values of the HOMO-LUMO gap (ΔE_{gap}). Because of soft molecules have lower polarizability and higher excitation energies, hard molecules are more likely to display Nonlinear Optical (NLO) activity. Furthermore, a molecule is more likely to have electronic transitions when ΔE is minimal. Theoretically, Glu-Ureido was dissolved in dichloromethane for UV-Vis electronic spectrum investigations. To applying B3LYP/6-311G(++,d,p) basis set, the TD-DFT method was employed to analyze the electronic spectrum. The primary Glu-Ureido contributions are displayed in Table 3 together with their oscillator strengths (*f*), excitation energy (E), and wavelengths (*λ*).

Table 3. Theoretical absorption wavelength λ (nm) and excitation energies E(eV) of Glu-Ureido employing 6-311++g(d,p) basis set and B3LYP functional.

SN	Electronic Transitions (Molecular Orbitals Involved)	Energy (eV)	Oscillatory Strength (*f*)	Calculated λ_{max} in nm (B3LYP)
01	HOMO → LUMO	5.91	0.0036	222.68
02	HOMO-1 → LUMO	6.42	0.0036	222.68

03	HOMO-2 → LUMO	7.07	0.0036	222.68
04	Urea	7.36	--	--
05	2M4NA (2-methyl-4-nitroaniline)	6.36	--	--

The HOMO-LUMO gap values of the Glu-Ureido are listed in Table 3 and compared with the corresponding 2M4NA and urea energy(eV) values, which are used as references. The HOMO and LUMO graphs were plotted and shown in Figure 2. The Table 3 predicts that, the first transition of the HOMO-LUMO energy gap will occur at 5.91 eV and exhibits higher chemical stability in comparison to the standard. The value of Glu-Ureido chemical moiety is considered to exhibit lower values than urea (7.36 eV) and 2M4NA (6.36 eV) which indicate that most reactive from the electronic point of view. In HOMO-LUMO plots, the positive phases are displayed in yellow, and the negative phases are shown in green.
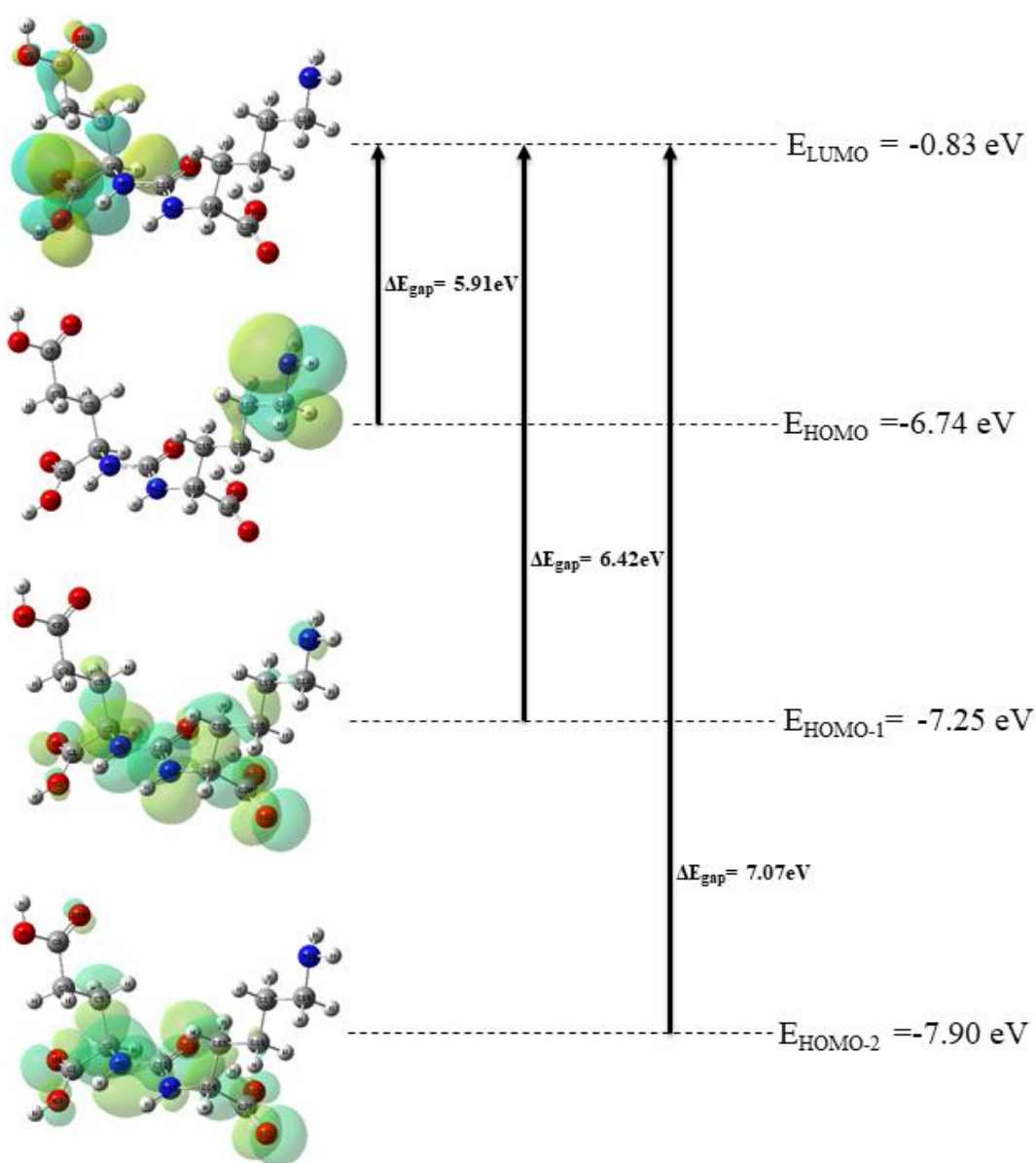
Figure 2. Molecular orbitals (HOMO→LUMO, HOMO-1→LUMO and HOMO-2→LUMO) of Glu-Ureido at the B3LYP/ 6-311++g(d,p) basis set.

Chem. Proc. **2024**, *6*, x FOR PEER REVIEW

6 of 10

3.3. Molecular Electrostatic Potential Surface (MESP)

Molecular electrostatic potential surfaces (MESP) have been utilized to identify and explain the regions of nucleophilic and electrophilic. To elucidate the colour changes between the electron-poor and electron-rich regions, the MESP of the Glu-Ureido chemical structure has been generated. The Glu-Ureido's MESP is colour-coded between −0.102 and 0.102 a.u. The strongest electron attraction is shown by the blue regions in Figure 3, whereas the electron repulsion is indicated by the red regions. The figure illustrates that the blue areas are electron-poor zones, especially those surrounding the hydrogens in the urea linkage. In contrast, the red regions indicate electron-rich areas developing around the oxygen atoms of the carboxylic group.
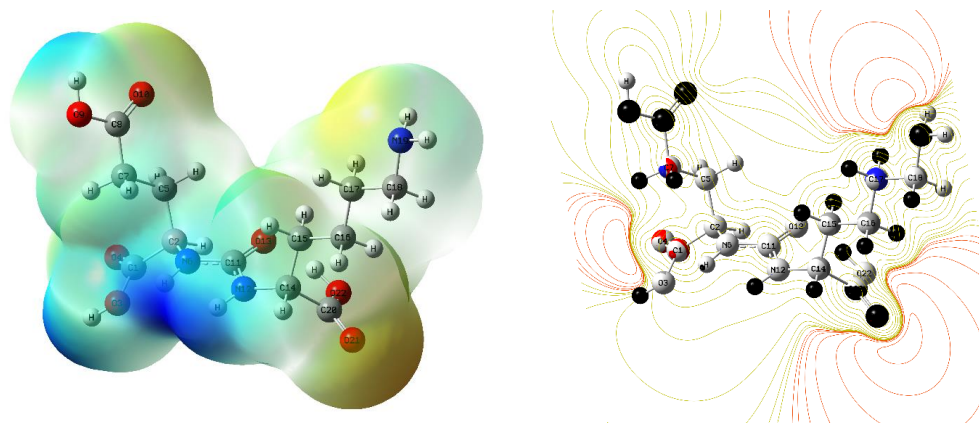
Figure 3. Molecular electrostatic surface potential (MESP) analysis of Glu-Ureido chemical moiety.

3.4. Global Reactivity Descriptors

The terms used to explain the global reactivity descriptor are global hardness (η), electronegativity (χ), chemical potential (μ) and electrophilicity index (ω) etc. These are utilized in the computation of the molecular systems' chemical reactivity and site selectivity by DFT calculation. The global reactivity descriptors values can be calculated by using Koopman's theorem by HOMO and LUMO energies using the following formula and listed in Table 4 [20–24].

$$Ionization\ potential\ (IP) = -\varepsilon_{HOMO} \tag{1}$$

$$Electron\ affinity\ (EA) = -\varepsilon_{LUMO} \tag{2}$$

$$Electronegativity\ (\chi) = -\frac{1}{2}(\varepsilon_{LUMO} + \varepsilon_{HOMO}) \tag{3}$$

$$Global\ hardness\ (\eta) = \frac{1}{2}(\varepsilon_{LUMO} - \varepsilon_{HOMO}) \tag{4}$$

$$Chemical\ potential\ (\mu) = -\chi = \frac{1}{2}(\varepsilon_{LUMO} + \varepsilon_{HOMO}) \tag{5}$$

$$Electrophilicity\ index\ (\omega) = \frac{\mu^2}{2\eta} \tag{6}$$

$$(\triangle N_{\max}) = \frac{-\mu}{\eta} \tag{7}$$

Table 4. Global reactive descriptor values for Glu-Ureido chemical moiety.

Compound	ε_{HOMO}	ε_{LUMO}	ε_{LUMO}-ε_{HOMO}	IP	EA	χ	η	μ	ω	δN_{max}
Glu-Ureido	−6.74	−0.83	5.91	6.74	0.83	3.78	2.95	−3.78	2.42	1.28

3.5. Nonlinear Optical Properties

The high-potential components of non-linear optical (NLO) features, which have many uses in physical chemistry. A molecule can be distinguished by its dipole moment, polarizability and hyperpolarizability in an applied electric field. The total static dipole moment (μ_{tot}), mean first-order hyperpolar-izability (β_{tot}), and average linear polarizability (α_{tot}) are defined using the x, y and z components and define as follows:

$$dipole\ moment\ (\mu_{tot}) = (\mu^2_{\,x} + \mu^2_{\,y} + \mu^2_{\,z})^{1/2} \tag{8}$$

$$polarizibality\ (\alpha_{tot}) = \frac{1}{3}(\alpha_{xx} + \alpha_{yy} + \alpha_{zz}) \tag{9}$$

$$hyperpolarizability\ (\beta_{tot}) = [(\beta_{xxx} + \beta_{xyy} + \beta_{xzz})^2 + (\beta_{yyy} + \beta_{yxx} + \beta_{yzz})^2 + (\beta_{zzz} + \beta_{zxx} + \beta_{zyy})^2]^{1/2} \tag{10}$$

Therefore, the whole molecule polarizability (αtot) and its components, the total molecular dipole moment (μtot) and the first-order hyperpolarizability (βtot), were computed to determine the NLO behaviour of the Glu-Ureido chemical moiety. It was discovered that the electronic dipole moment (μ_{tot}) was 2.54 Debye and polarizability was found 137.927 esu whereas first hyperpolarizability value of Glu-Ureido was found to be 144.328 esu. The high hyperpolarizability value of the system indicates a relationship between intramolecular charge transfer and its NLO property (Table 5).

Table 5. Dipole moment (μ_{total}), polarizability (α_{total}) and hyperpolarizability (β_{total}) of Glu-Ureido.

Dipole Moment		Polarizability		Hyperpolarizability	
μ_x	1.290	α_{xx}	224.385	β_{xxx}	−3.811
μ_y	0.674	α_{yy}	1.813	β_{yyy}	−17.940
μ_z	−2.083	α_{zz}	187.583	β_{zzz}	104.721
μ_{tot}(D)	2.54	α_{xy}	1.360	β_{xyy}	33.355
		α_{xz}	5.798	β_{xxy}	24.754
		α_{yz}	166.295	β_{xxz}	43.385
		α_0 **(esu)**	137.927	β_{xzz}	−33.447
				β_{yzz}	20.029
				β_{yyz}	−6.349
				β_{xyz}	−71.173
				β_0 **(esu)**	144.328

4. Conclusions

This study explores the structural and electronic properties of the Glu-Ureido chemical moiety using quantum chemistry simulations based on DFT calculations. To assess it's chemical stability, HOMO-LUMO plots were analyzed, revealing the energy gap between the highest occupied molecular orbital (HOMO) and the lowest unoccupied molecular orbital (LUMO), which indicates the reactive sites within the Glu-Ureido template.

The MESP surfaces were employed to identify electronic-poor and electronic-rich regions, providing insights into the surface morphology. The small energy gap between HOMO and LUMO confirmed charge transfer, suggesting that the compound has lower kinetic stability and higher chemical reactivity, making it more likely to exhibit NLO activity. Additionally, the calculated first-order hyperpolarizability and dipole moment values further supported the active NLO behavior of the Glu-Ureido moiety.

Author Contributions: M.F.: Investigation, methodology, data correction, original draft, editing, communication; V.P.: data correction, editing; M.D.: Supervision, review and editing. All authors have read and agreed to the published version of the manuscript.

Institutional Review Board Statement: Not applicable.

Informed Consent Statement: Not applicable.

Data Availability Statement: Data are contained within the article.

Conflicts of Interest: The authors declare no conflict of interest.

References

1. Young, V.R.; Ajami, A.M. Glutamate: An Amino Acid of Particular Distinction. *J. Nutr.* **2000**, *130*, 892S–900S. https://doi.org/10.1093/jn/130.4.892S.
2. Wüstemann, T.; Bauder-Wüst, U.; Schäfer, M.; Eder, M.; Benesova, M.; Leotta, K.; Kratochwil, C.; Haberkorn, U.; Kopka, K.; Mier, W. Design of Internalizing PSMA-Specific Glu-Ureido-Based Radiotherapeuticals. *Theranostics* **2016**, *6*, 1085–1095. https://doi.org/10.7150/thno.13448.
3. Kopka, K.; Benešová, M.; Bařinka, C.; Haberkorn, U.; Babich, J. Glu-Ureido–Based Inhibitors of Prostate-Specific Membrane Antigen: Lessons Learned During the Development of a Novel Class of Low-Molecular-Weight Theranostic Radiotracers. *J. Nucl. Med.* **2017**, *58* (Suppl. 2), 17S–26S. https://doi.org/10.2967/jnumed.116.186775.
4. Lowe, P.T.; Dall'Angelo, S.; Fleming, I.N.; Piras, M.; Zanda, M.; O'Hagan, D. Enzymatic Radiosynthesis of a ¹⁸ F-Glu-Ureido-Lys Ligand for the Prostate-Specific Membrane Antigen (PSMA). *Org. Biomol. Chem.* **2019**, *17*, 1480–1486. https://doi.org/10.1039/C8OB03150A.
5. Young, J.D.; Ma, M.T.; Eykyn, T.R.; Atkinson, R.A.; Abbate, V.; Cilibrizzi, A.; Hider, R.C.; Blower, P.J. Dipeptide Inhibitors of the Prostate Specific Membrane Antigen (PSMA): A Comparison of Urea and Thiourea Derivatives. *Bioorg. Med. Chem. Lett.* **2021**, *42*, 128044. https://doi.org/10.1016/j.bmcl.2021.128044.
6. Hyväkkä, A.; Virtanen, V.; Kemppainen, J.; Grönroos, T.J.; Minn, H.; Sundvall, M. More Than Meets the Eye: Scientific Rationale behind Molecular Imaging and Therapeutic Targeting of Prostate-Specific Membrane Antigen (PSMA) in Metastatic Prostate Cancer and Beyond. *Cancers* **2021**, *13*, 2244. https://doi.org/10.3390/cancers13092244.
7. Sheehan, B.; Guo, C.; Neeb, A.; Paschalis, A.; Sandhu, S.; de Bono, J.S. Prostate-Specific Membrane Antigen Biology in Lethal Prostate Cancer and Its Therapeutic Implications. *Eur. Urol. Focus.* **2022**, *8*, 1157–1168. https://doi.org/10.1016/j.euf.2021.06.006.
8. Nikfarjam, Z.; Bavi, O.; Amini, S.K. Potential Effective Inhibitory Compounds against Prostate Specific Membrane Antigen (PSMA): A Molecular Docking and Molecular Dynamics Study. *Arch. Biochem. Biophys.* **2021**, *699*, 108747. https://doi.org/10.1016/j.abb.2020.108747.
9. Pastorino, S.; Riondato, M.; Uccelli, L.; Giovacchini, G.; Giovannini, E.; Duce, V.; Ciarmiello, A. Toward the Discovery and Development of PSMA Targeted Inhibitors for Nuclear Medicine Applications. *Curr. Radiopharm.* **2020**, *13*, 63–79. https://doi.org/10.2174/1874471012666190729151540.
10. Liolios, C.; Patsis, C.; Lambrinidis, G.; Tzortzini, E.; Roscher, M.; Bauder-Wüst, U.; Kolocouris, A.; Kopka, K. Investigation of Tumor Cells and Receptor-Ligand Simulation Models for the Development of PET Imaging Probes Targeting PSMA and GRPR and a Possible Crosstalk between the Two Receptors. *Mol. Pharm.* **2022**, *19*, 2231–2247. https://doi.org/10.1021/acs.molpharmaceut.2c00070.
11. Hanwell, M.D.; Curtis, D.E.; Lonie, D.C.; Vandermeersch, T.; Zurek, E.; Hutchison, G.R. Avogadro: An Advanced Semantic Chemical Editor, Visualization, and Analysis Platform. *J. Cheminform.* **2012**, *4*, 17. https://doi.org/10.1186/1758-2946-4-17.
12. Kohn, W.; Sham, L.J. Self-Consistent Equations Including Exchange and Correlation Effects. *Phys. Rev.* **1965**, *140*, A1133–A1138. https://doi.org/10.1103/PhysRev.140.A1133.
13. Becke, A.D. Density-Functional Thermochemistry. I. The Effect of the Exchange-Only Gradient Correction. *J. Chem. Phys.* **1992**, *96*, 2155–2160. https://doi.org/10.1063/1.462066.
14. Lee, C.; Yang, W.; Parr, R.G. Development of the Colle-Salvetti Correlation-Energy Formula into a Functional of the Electron Density. *Phys. Rev. B* **1988**, *37*, 785–789. https://doi.org/10.1103/PhysRevB.37.785.
15. Frisch, M.J. Gaussian. 2009.

16. Frisch, M.J.; Trucks, G.W.; Schlegel, H.B.; Scuseria, G.E.; Robb, M.A.; Cheeseman, J.R.; Scalmani, G.; Barone, V.; Mennucci, B.; Petersson, G.A.; et al. *Gaussian 09*; Gaussian: Wallingford, CT, USA, 2009; pp. 150–166.

17. Kleinman, D.A. Nonlinear Dielectric Polarization in Optical Media. *Phys. Rev.* **1962**, *126*, 1977–1979. https://doi.org/10.1103/PhysRev.126.1977.

18. Pipek, J.; Mezey, P.G. A Fast Intrinsic Localization Procedure Applicable for ab initio and Semiempirical Linear Combination of Atomic Orbital Wave Functions. *J. Chem. Phys.* **1989**, *90*, 4916–4926. https://doi.org/10.1063/1.456588.

19. Krishnakumar, V.; Keresztury, G.; Sundius, T.; Ramasamy, R. Simulation of IR and Raman Spectra Based on Scaled DFT Force Fields: A Case Study of 2-(Methylthio)Benzonitrile, with Emphasis on Band Assignment. *J. Mol. Struct.* **2004**, *702*, 9–21. https://doi.org/10.1016/j.molstruc.2004.06.004.

20. Gritsenko, O.V. Koopmans' Theorem and Its Density-Functional-Theory Analog Assessed in Evaluation of the Red Shift of Vertical Ionization Potential upon Complexation. *Chem. Phys. Lett.* **2018**, *691*, 178–180. https://doi.org/10.1016/j.cplett.2017.11.019.

21. Pearson, R.G. Absolute Electronegativity and Hardness: Applications to Organic Chemistry. *J. Org. Chem.* **1989**, *54*, 1423–1430. https://doi.org/10.1021/jo00267a034.

22. Parr, R.G.; Szentpály, L. v.; Liu, S. Electrophilicity Index. *J. Am. Chem. Soc.* **1999**, *121*, 1922–1924. https://doi.org/10.1021/ja983494x.

23. Chattaraj, P.K.; Giri, S. Stability, Reactivity, and Aromaticity of Compounds of a Multivalent Superatom. *J. Phys. Chem. A* **2007**, *111*, 11116–11121. https://doi.org/10.1021/jp0760758.

24. Padmanabhan, J.; Parthasarathi, R.; Subramanian, V.; Chattaraj, P.K. Electrophilicity-Based Charge Transfer Descriptor. *J. Phys. Chem. A* **2007**, *111*, 1358–1361. https://doi.org/10.1021/jp0649549.